The Astrophysical Journal, 648:1247–1255, 2006 September 10

SOLAR SOURCE REGIONS FOR ^{3}He-RICH SOLAR ENERGETIC PARTICLE EVENTS IDENTIFIED USING IMAGING RADIO, OPTICAL, AND ENERGETIC PARTICLE OBSERVATIONS

M. Pick,[1] G. M. Mason,[2] Y.-M. Wang,[3] C. Tan,[1,4] and L. Wang[5]

Received 2005 October 4; accepted 2006 May 15

ABSTRACT

We have identified the sources of six impulsive ^{3}He-rich solar energetic particle events using imaging radio, optical, and energetic ion and electron data, together with calculated coronal fields obtained from extrapolating photospheric magnetograms using a potential field source surface (PFSS) model. These events were all studied in 2006 by Wang et al., who identified the particle sources as typically small, flaring active regions lying next to a coronal hole containing Earth-directed open field lines, located between W33° and W65°. By introducing radio imaging data we were able in one case to conclusively identify which of two simultaneous EUV jets was associated with the particle source. In addition, type III radio burst and energetic electron data introduced in this study constrain the injection times much more accurately than possible with low-energy ion data used in Wang et al. These new observations confirm the source identifications of Wang et al. and remove many of the remaining uncertainties. All of these events were associated with narrow, fast coronal mass ejections (CMEs), which are unusual for ^{3}He-rich solar energetic particle (SEP) events. Although the CMEs generally were ejected in directions well off the ecliptic plane, the PFSS calculations show the presence of magnetic field lines that made it possible for the energetic particle to quickly reach Earth. Some of these impulsive events were observed during periods in which ^{3}He was observed continuously over several days.

Subject headings: Sun: coronal mass ejections (CMEs) — Sun: radio radiation — Sun: X-rays, gamma rays

1. INTRODUCTION

In 1970 Hsieh & Simpson (1970) first observed solar energetic particle (SEP) events with unusually high abundances of ^{3}He. Following these early observations, it was discovered that events showing the highest ^{3}He enhancements were small particle events with ^{3}He/^{4}He ratio up to $\sim$1 (e.g., Garrard et al. 1973; Serlemitsos & Balasubrahmanyan 1975), enormously higher than the typical value of a few times 10^{-4} found in the solar corona or solar wind (Geiss & Reeves 1972). Further studies revealed that ^{3}He-rich flares were associated with impulsive energetic electron events and type III radio emission (Reames et al. 1985, 1988). Although many of these events are associated with "impulsive" X-ray flares, many ^{3}He-rich particle events are observed at 1 AU that have no identified source activity at the Sun. We note that these impulsive events have distinct characteristics that generally separate them from large coronal mass ejection (CME) shock-associated "gradual" events whose ion composition does not show such large anomalies (for a recent review, see Reames 1996).

Recently, Kahler et al. (2001) made the surprising discovery that a fast, narrow ($\sim$20°) CME was associated with the ^{3}He-rich SEP event of 2000 May 1. Pick et al. (2003) showed that this event was also associated with a series of type III–like radio sources that moved outward with a velocity comparable to the projected CME velocity of 1340 $\pm$ 70 km s^{-1} and that the outward-moving metric radio sources fit well within the height-time curve of the CME. Kahler et al. (2001) found several additional cases of narrow CME associations with impulsive events, making these cases quite unusual, since hundreds of impulsive SEP events have been observed. Adopting the Shimojo & Shibata (2000) model of impulsive flares, in which jets or plasmoids are ejected upward from magnetic reconnection sites, Kahler et al. suggested that such jets could be appear as faint and narrow CMEs in unusually energetic impulsive events.

Wang et al. (2006, hereafter Paper I) examined 25 ^{3}He-rich SEP events, combining imaging observations with a potential field source surface (PFSS) model to extrapolate photospheric magnetograph measurements to the corona. It was found that in virtually all cases, the impulsive particle event source was next to a western hemisphere coronal hole containing Earth-directed field lines. The sources were typically small, flaring active regions similar to jet-producing regions studied in white light and EUV by Wang & Sheeley (2002). The activity in these regions is believed to be caused by flux emergence and cancellation, causing the active region fields to reconnect with the overlying open field lines releasing trapped energy in the form of jetlike ejections (Shimojo & Shibata 2000; Wang & Sheeley 2002).

The technique of Paper I is subject to uncertainties due to the uncertainties in deriving ion injection times at the Sun, and also the limitations of the static PFSS model. In order to reduce these uncertainties, we have used energetic electron, type III burst observations, and imaging radio data to constrain the timing and locate the emission regions in the corona. In particular, the radio spectral observations covering a large frequency range make it possible to trace the relationship between the coronal and interplanetary emissions. The radio imaging observations provide the locations of the radio sources in the corona at decimeter-meter wavelengths. Taken together with the PFSS extrapolations, X-ray, EUV, and white-light data of the type used by Paper I, these new observations greatly reduce possible uncertainties in the source identification. While the associated jets and CMEs

[1] Observatoire de Paris, LESIA, UMR 8109 (CNRS), 5 Place Jules Janssen, F-92195 Meudon Cedex, France; monique.pick@obspm.fr.
[2] Applied Physics Laboratory, Johns Hopkins University, Laurel, MD 20723-6099.
[3] E. O. Hulburt Center for Space Research, Naval Research Laboratory, Washington, DC 20375-5352.
[4] National Astronomical Observatory, Chinese Academy of Science, 100012 Beijing, China.
[5] Space Science Laboratory, University of California, Berkeley, CA 94720.

in these events are often directed well off the ecliptic plane, the PFSS calculations show that the source regions have magnetic connection to the ecliptic plane, providing a path for the energetic particles to reach Earth.

2. OBSERVATIONS

2.1. *Instrumentation*

The low-energy ion data used here are from the Ultra Low Energy Isotope Spectrometer (ULEIS; Mason et al. 1998) on the *Advanced Composition Explorer* (*ACE*) spacecraft, which was launched into a halo orbit around the sunward Lagrangian point in 1997 (Stone et al. 1998). ULEIS covers the energy range $\sim$0.2–10 MeV nucleon^{-1} and identifies periods when ^{3}He is enriched. Electron observations were made using sensors in the three-dimensional plasma (3DP) investigation on the *Wind* spacecraft (Lin et al. 1995). For the current study, electrons over the range of a few to a few hundred keV were used.

Imaging radio data were obtained from the Nançay radioheliograph (NRH), which provided images of the radio bursts in the range 432–150 MHz (Kerdraon & Delouis 1997). Spectral data in the frequency range 20–70 MHz were obtained by the Nançay Decameter Array (DAM; Lecacheux 2000). Below 14 MHz, we used data from the Radio and Plasma Wave Investigation on the *Wind* Spacecraft (WAVES; Bougeret et al. 1995), and in the range 800–40 MHz we used data from the Tremsdorf Observatory of Solar Radioastronomy (OSRA) instrument (Mann et al. 1992). Solar magnetic field data were obtained from the National Solar Observatory Kitt Peak magnetograms and also from the Michelson Doppler Imager (MDI) on the *Solar and Heliospheric Observatory* (*SOHO*) spacecraft (Scherrer et al. 1995). EUV imaging observations at 195 Å were obtained with the *SOHO* Extreme Ultraviolet Imaging Telescope (EIT; Delaboudinière et al. 1995). White-light observations of the corona were obtained with the *SOHO* Large Angle and Spectrometric Coronagraph (LASCO; Brueckner et al. 1995).

2.2. *Event Selection and Source Determination*

We searched for ^{3}He-rich events for which the ion injection took place during the daily period (roughly 08:00–16:00 UT) when the NRH was imaging the Sun, and when there was little energetic particle background from preceding large SEP events. Table 1 lists properties of the six events identified for this study. Columns (3)–(6) of the table list the parent Hα flare properties from the NOAA SEL Web site, except for the 2000 May 1 event, which was identified in X-rays only (see discussion in Kahler 2001). Note that three of the events have no parent Hα flare association, which is typical of ^{3}He-rich events. Columns (7)–(9) list the EIT event type and properties from Paper I. Energetic particle injection times are in columns (10)–(12), with column (11) showing >15 MeV proton injection times from the study of Klein & Posner (2005). The energetic particle injection times are obtained by subtracting interplanetary propagation times from the observed rise time at Earth; these corrections are about 1 hr for 15 MeV protons and 13 keV electrons, and 6 hr for the low-energy ions. The fact that several of these events produced >15 MeV protons indicates that these events were more energetic than typical impulsive events (see also Kahler 2001). Columns (13)–(15) list the type III onset/end times, and low-energy ^{3}He/^{4}He and Fe/O ratios. It can be seen that all of the events were ^{3}He-rich and also had large Fe/O ratios typical of this type of SEP event.

Figure 1 shows an example of the energetic particle data used for deriving injection times. The left panel is a spectrogram plot of 1/(ion speed) versus arrival time for ULEIS 10–70 amu ions for the period that contains event 3 in Table 1. The energy range of the ion data shown is roughly 50 keV–2 MeV nucleon^{-1} (corresponding respectively to 13 and 2 hr AU^{-1} speed). The slanted lines in the panel show the arrival times at Earth orbit for particles injected at the Sun and traveling along a nominal 1.2 AU Archimedes spiral path to Earth. The arrow points to the event 3 ion arrivals, where it can be seen that the leading edge is nearly parallel to the slanted lines, indicating that there was little or no scattering in the interplanetary medium for these ions. The tip of the arrow points to the injection time at the Sun determined by extrapolating the leading edge down to zero flight time, approximately at 15:00 UT. This technique of deriving the ion injection time is subject to typical uncertainties of $\pm$1 hr due to the lack of sharpness of the leading edge of the spectrogram, and also the unknown actual length of the interplanetary magnetic field (IMF) line spiral. For this event and event 4, this uncertainty has been lowered some by a more detailed fit that looks at a number different ion energies and derives an IMF field length as well as an injection time (see Wang et al. 2005). Even with this improved analysis, the injection time uncertainties are large.

The right panel of Figure 1 shows impulsive electrons observed on the *Wind* spacecraft for this period. Note that the timescale of this figure is greatly expanded in comparison to the left panel (7 vs. 48 hr). The electrons show clear velocity dispersion. By carefully fitting the electron onsets in several energy channels, Wang et al. (2005) derived an injection time of 14:13 $\pm$ 00:02 for this event, after adding 500 s to account for the photon travel time for use in comparing with the radio data. The large improvement in accuracy for the electron data is due primarily to their high speed (12 minute flight time at the highest energies), and so the uncertainties arising from the IMF length produce small uncertainties in injection time. Note also from the electron plot that for this event there is no other activity for 2 or more hours before or after the injection.

Continuing with event 3, Figure 2 shows the radio data. For the left side of the figure, the top two panels show frequency versus time; there are multiple features in the DAM and NRH panels, while the lower frequency WAVES data, which have a cadence of 60 s, show only a single type III burst. The bottom two panels show one-dimensional brightness plots from the NRH, obtained by integrating the images in one dimension and displaying the result as a function of time. In these panels, the vertical axis gives the east-west and north-south position in solar radii for a coordinate system centered on the solar disk. For the multiple bursts seen in the DAM and NRH plots, there is no way to tell from the present data whether or not the electrons associated with each burst escaped and propagated to Earth; since we see electrons at Earth particles from at least one burst propagated to Earth, we cannot tell which burst it came from, and perhaps particles from several or all of the bursts propagated to Earth. For this reason, in Table 1 the type III burst times associated with this and the other events cover several minutes. The shaded boxes at the bottom left show the type III burst onset/end times, the $\geq$13 keV electron, and >15 MeV proton injection times from the table. These times overlap within accuracies of a few minutes; however, the deduced low-energy ion injection time is significantly later, which is discussed below. The right panel of Figure 2 shows the radio image in the southwestern solar quadrant for one of the early type III bursts.

In the top left panel of Figure 3 we now combine the radio imaging data with the LASCO C2 coronagraph image superposed with an EIT Fe XII λ195 image made close to the times of the energetic electron injection and type III bursts. The EIT

TABLE 1

^{3}HE-RICH SOLAR ENERGETIC PARTICLE EVENT PROPERTIES

		Hα FLARE[a]				EIT EVENT[a] (UT ± 1 minute)			ENERGETIC PARTICLE INJECTION TIME			TYPE III BURST ONSET END	ION COMPOSITION[b]	
NUMBER	START DAY	Max Time (UT)	IMP	Location (deg)	NOAA USAF Region	Type	Location (deg)	Time (UT)	Low–Energy Ions	>15 MeV Protons	≥13 keV Electrons	(UT)	^{3}He/^{4}He	Fe/O
(1)	(2)	(3)	(4)	(5)	(6)	(7)	(8)	(9)	(10)	(11)[c]	(12)	(13)	(14)	(15)
1.....	2000 May 1	10:24	...	N20, W54[d]	8971[d]	λ195 flare	N20, W49	10:24	10:05 ± 60	10:24 ± 3	10:23 ± 2	10:19−10:25[e]	0.062 ± 0.006	2.22 ± 0.15
2.....	2002 Oct 5	11:52	SF	N9, W53	10138	λ195 flare/jet	N09, W65	12:12	13:00 ± 60	12:16 ± 3	12:17 ± 1[f]	12:13−12:21	0.63 ± 0.09	1.77 ± 0.24
3.....	2002 Oct 20[g]	14:15	SF	S13, W63	10154	λ195 flare/jet	N09, W65	14:24	14:55 ± 33[h]	14:20 ± 5	14:13 ± 2	14:10−14:13	1.59 ± 0.08	2.57 ± 0.31
4.....	2002 Dec 12	...	...	N15, W50[i]	10212[i]	λ195 flare/jet	N14, W35	12:48	13:37 ± 62[h]	12:41 ± 3	12:43 ± 1	12:35−>12:42[j]	0.48 ± 0.05	1.84 ± 0.32
5.....	2003 Mar 2	...	...	...	...	λ195 flare/jet	S15, W25	14:24	[k]	...	14:27 ± 9	14:12−14:20	0.65 ± 0.07	0.87 ± 0.19
6.....	2003 Mar 17	10:14	SF	S16, W33	10314	λ195 flare	S17, W35	10:14	10:00 ± 60	...	10:13 ± 2	10:10−10:16	0.18 ± 0.02	0.56 ± 0.18

[a] Flare and EIT events from Paper I, except for 2000 May 1 event (see also Mason et al. 2004); region and flare importance are from http://www.ngdc.noaa.gov/stp/SOLAR/ftpsolarflares.html.

[b] Ion composition at 385 keV nucleon^{-1} for event 1; at 400–600 keV nucleon^{-1} for others.

[c] From Klein & Posner (2005).

[d] No Hα flare observed; this identification is from Kahler et al. (2001).

[e] From Pick et al. (2003).

[f] From the *ACE* Electron, Proton, and Alpha Monitor (EPAM) (Gold et al. 1998).

[g] The 2002 October 20 event had two impulsive ion injections. Paper I studied the event starting at 05:29 UT; the event in present table was the second impulsive event, which occurred during the operating hours of the NRH. Flare identification is from NOAA site (see note a); EIT event time is from Paper I (Fig. 15).

[h] From Wang et al. (2005).

[i] No Hα flare observed; this identification is based on observed EIT jet (see text).

[j] For 2002 December 12, spectral identification between 200 and 90 MHz was not possible due to very high radio interference.

[k] The 2000 March 3 event did not show velocity dispersion for ions; the entire period March 2 18:00 UT through March 3 18:00 UT was enriched with energetic ^{3}He, consistent with the injection times shown for electrons and a 6 hr propagation time for 400 keV nucleon^{-1} ions to *ACE* along a 1.2 AU spiral IMF line.

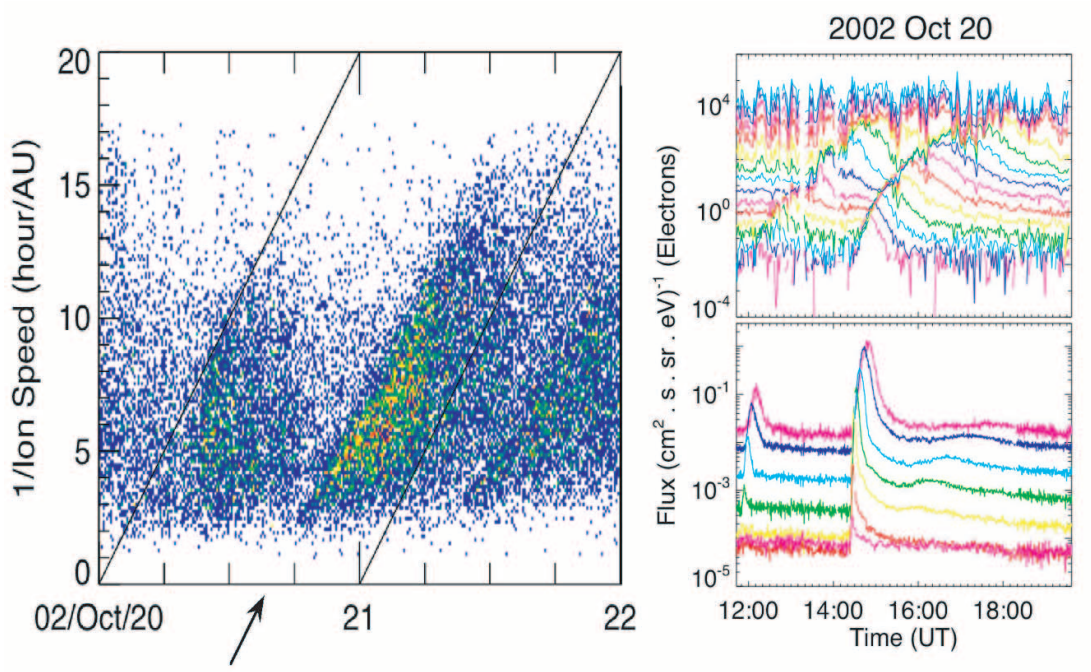

FIG. 1.—*Left*: Spectogram of 1/speed vs. arrival times of 10–70 amu ions for the period 2002 October 20–22. Slanted lines show arrival times for particles traversing 1.2 AU IMF spirals with no scattering. Arrow marks approximate injection time of event 3. *Right*: Impulsive electron intensities, showing clear velocity dispersion. Energy range for top panel is ~0.14–28 keV; range for bottom panel is ~27–510 keV. Flight time for the highest energy electrons along a 1.2 AU spiral with no scattering is about 12 minutes.

image is made by taking the difference between two successive images in order to enhance changing features; the two images are typically spaced by 12 minutes. There are two virtually simultaneous brightenings in the difference image; the radio imaging data of the type III burst, marked by a white asterisk, makes it possible to identify the westernmost brightening as the one associated with the particle event (*arrow*). Also, a narrow CME is associated with this event, moving to the southwest.

The top right panel of Figure 3 shows the solar magnetic field at the disk, where black, dark gray, light gray, and white

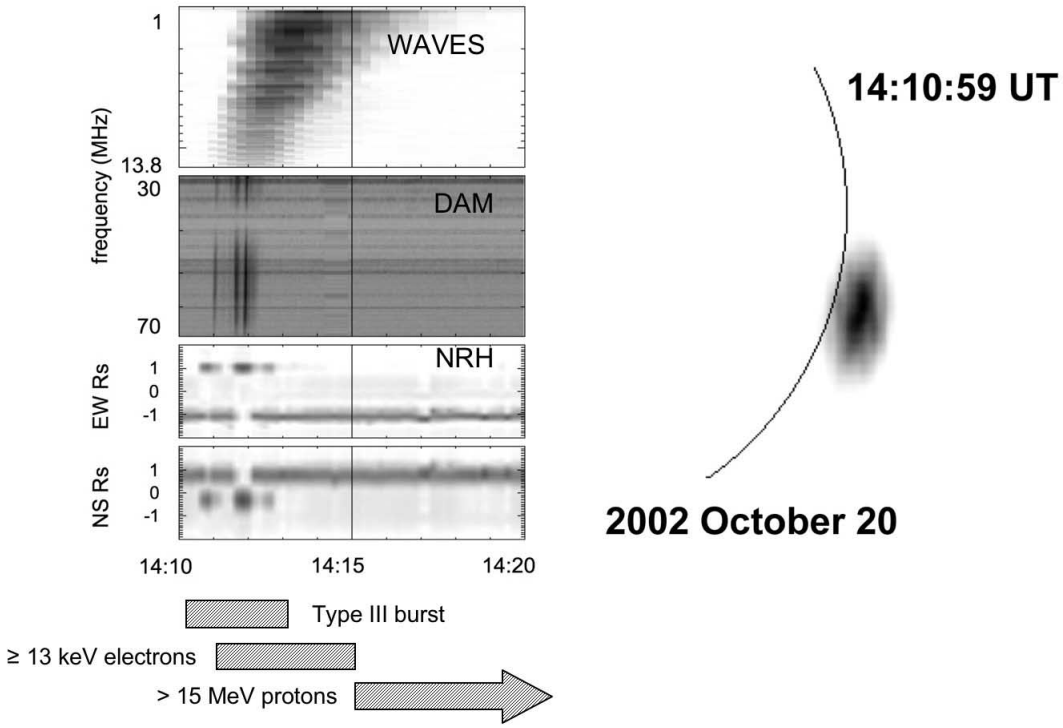

FIG. 2.—*Top left*: Type III radio bursts observed the WAVES and DAM radiospectrographs for the event shown in Fig. 1. *Bottom left*: 164 MHz NRH plots of the east-west and north-south positions of radio sources in a coordinate system centered on the solar disk. *Shaded boxes*: Type III burst onset/end time, and energetic electron and proton injection times from Table 1. *Right*: Image of the western hemisphere source at 14:10:59 UT.

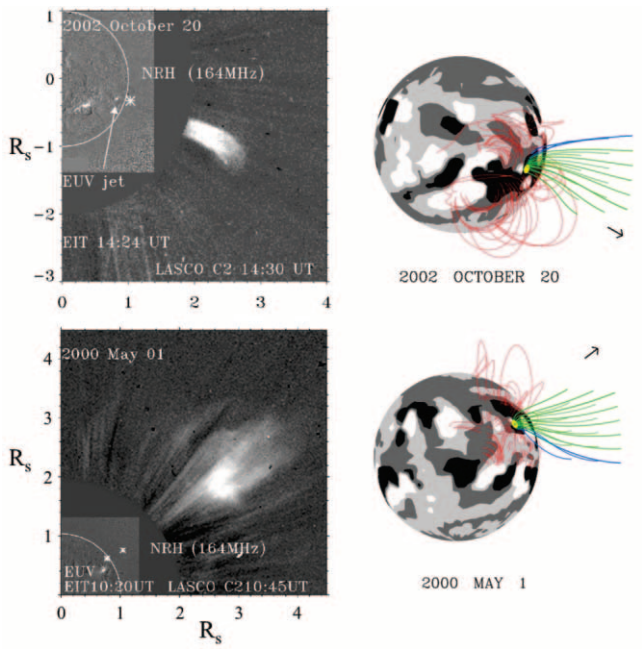

FIG. 3.— Composite data for the 2002 October 20 event and 2000 May 1 event. *Top left*: EIT difference image with arrow pointing to jet and white asterisk marking location of NRH 164 MHz radio source; narrow CME is visible in white-light LASCO C2 data. *Top right*: Solar disk showing magnetic field regions coded in black, gray, and white (see text). PFSS calculation shows closed field lines (*red*), open field (*green*), and open field with access to the ecliptic plane (*blue*). Yellow dot near source of open field lines is the identified source location (see text). Field lines are shown only for the vicinity of the source. The black arrow in the right panel shows direction of CME motion. *Bottom*: 2000 May 1 (*left*) NRH source locations over solar disk and CME and (*right*) magnetic fields and source location.

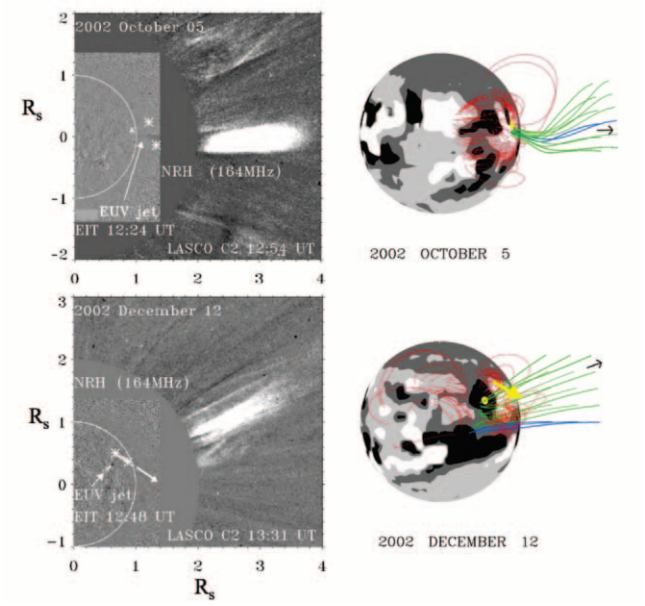

FIG. 4.— Same as Fig. 3. *Top*: 2002 October 5 event. *Bottom*: 2002 December 12 event. *Left*: Two asterisks and arrow show motion of the 164 MHz radio source, which is different from the direction of the white-light CME. *Right*: Thick yellow arrow shows the drift direction of radio source A (see text).

correspond respectively to photospheric fields $B_{\rm phot}$ of <-10 G, -10 G $< B_{\rm phot} < 0$, $0 < B_{\rm phot} < +10$ G, and $>+10$ G. The colored lines show the coronal field topology in the region of the particle event source, calculated with a PFSS model in which a current-free coronal field is extrapolated out to "source surface" at 2.5 Rs. In the figure, field lines that do not reach the source surface are closed (*red*), while those that reach the source surface are "open" to the interplanetary space off the ecliptic (*green*) or in the ecliptic (*blue*). The yellow dot in the figure marks the site of the particle event source deduced in Paper I, which was tentatively identified from the location of an Hα flare or EIT event (flare or ejection) within a few hours of the injection time and with location between $\sim$W20° and $\sim$W90°. Then, the type III burst timing, along with the radioheliograph location, gave additional information about the source identification. The fact that these source locations were on average within $\sim$4° of the PFSS calculated open field lines gives evidence that the field model is believable. The arrow in the right panel shows the direction of the CME, which had a projected speed of 723 km s^{-1} from linear fits to the LASCO C2 and C3 data. The right panels in Figures 3–5 are all from Paper I and are explained in more detail in that paper.

We now discuss the remaining events in Table 1. The bottom panels of Figure 3 show composite plots and PFSS model calculations for event 1. A noise storm near the equator was present before the event and is not shown in the figure. Note that the blue field lines in the bottom right panel show a magnetic connection between the source region and the ecliptic plane, which is not obvious given the direction of the CME (Paper I). The CME linear speed was 1360 km s^{-1}.[6] The metric radio images show a source moving outward at about the same position angle as the CME with a speed of about 1470 km s^{-1} (Pick et al. 2003). This event has been widely studied (e.g., Mason et al. 2000, 2002; Kahler 2001; Pick et al. 2003; Maia & Pick 2004; Klein & Posner 2005).

Figure 4 (*top*) shows event 2. There were two emitting regions at 164 MHz in this event, whose locations are shown with the white asterisks. One radio burst originates from a position

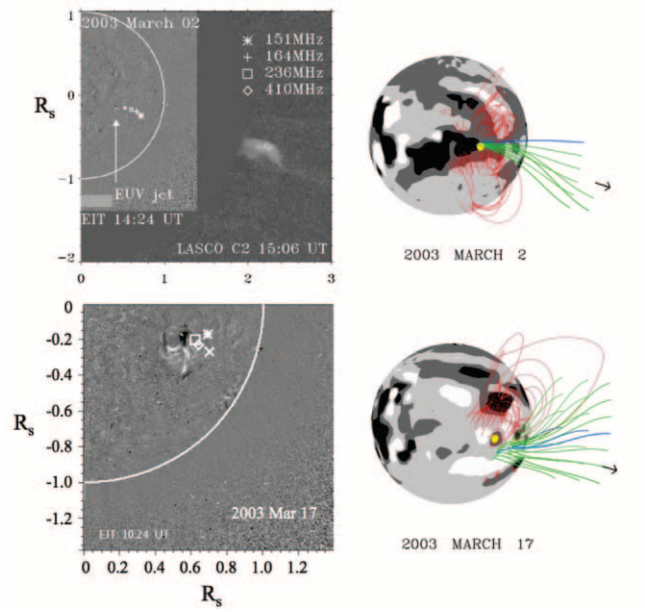

FIG. 5.— Same as Fig. 3, but for for 2003 March 2 and 2003 March 17 events. *Top left*: Multiple symbols (*asterisk*, *plus sign*, *square*, and *diamond*) show radio source location at 151–410 MHz. *Bottom left*: EIT difference image showing radio source at different frequencies; LASCO C2 data are not shown, since there was no clear CME association in this case (see text).

[6] See http://cdaw.gsfc.nasa.gov/CME_list/index.html.

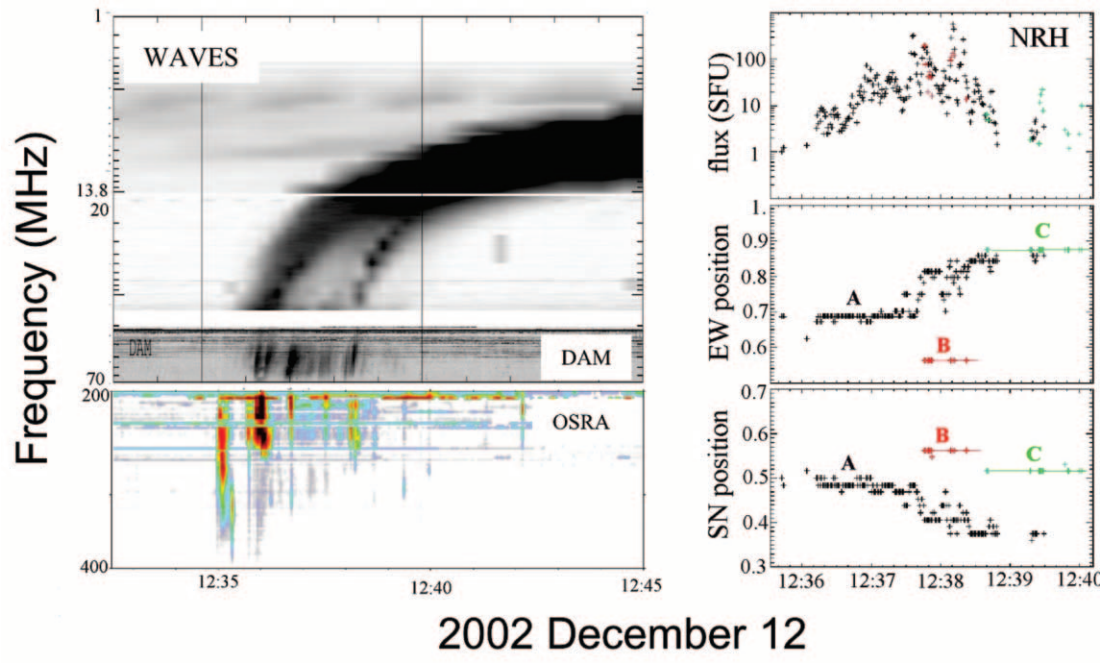

FIG. 6.—Complex radio spectral signatures in the 2000 December 12 event. *Left*: Type III radio emissions drifting from decimetric to kilometric wavelengths; note that the first bursts around 12:35 UT do not continue down to longer wavelengths. *Right, top to bottom*: Flux, east-west, and south-north position of the 164 MHz type III burst. The burst begins as a single source (A), which is reasonably stationary through 12:37:40 UT, after which it drifts southwest, and two other sources (B and C) appear.

south of the equator, with additional weak type III bursts detected at 12:18:00 and 12:20:40 UT. The other source is north of the equator and was in the same position as a permanent noise storm. The CME speed is 723 km s^{-1} for both the events in this figure. The bottom panels of Figure 4 show data for the 2000 December 12 event (No. 4). There was no Hα flare reported for this event. The deduced particle injection time near 12:41 UT was almost exactly midpoint between the two available EIT images at 12:36 and 12:48 UT. The figure shows a small jet near AR 10212 at N15°, W50°.

Figure 5 shows composite plots for events 5 and 6. In both left panels different symbols mark the type III burst locations for different frequencies. There was no jet observed for event 6; however, a λ195 flare was observed at the active region near the radio burst locations. The CME speed for this event, 386 km s^{-1}, is low; however, accounting for projection effects since the event was at ~W25°, a speed of ~900 km s^{-1} is reasonable. Event 6 is the only one that did not have a CME association, which is why the LASCO C2 observations are not shown. However, C2 did show a faint jetlike ejection entering the field of view at 10:54 UT, about 40 minutes after the electron injection time. This ejection might have been associated with this event.

2.3. *Complex Type III Radio Emission*

Several of the composite images in Figures 3–5 show that the type III bursts are not all simple point sources but rather show more complex behavior. We explore this more in event 4, whose type III radio burst patterns are shown in the left panels of Figure 6. Around 12:35 UT there are some high-frequency bursts that were barely detected by the NRH and are not seen by WAVES. These first bursts are also not seen in the lower frequency DAM panel, but note that due to interference there is a gap in the frequency range 200–90 MHz. The right panels show the 164 MHz intensity and east-west and north-south positions with 1 s time resolution covering about 5 minutes. For about the first 2 minutes, there is a single source (A), but after 12:37 UT it starts to drift to the southwest. While this was happening, two new sources (B and C) appeared. Higher frequency data showed different source locations as shown in Figure 7, where the sources A, B, and C are shown using different symbols to for each frequency. Source A was the only one detected at frequencies above 236 MHz. At the onset it is between two active regions (AR 10231 at N15°,

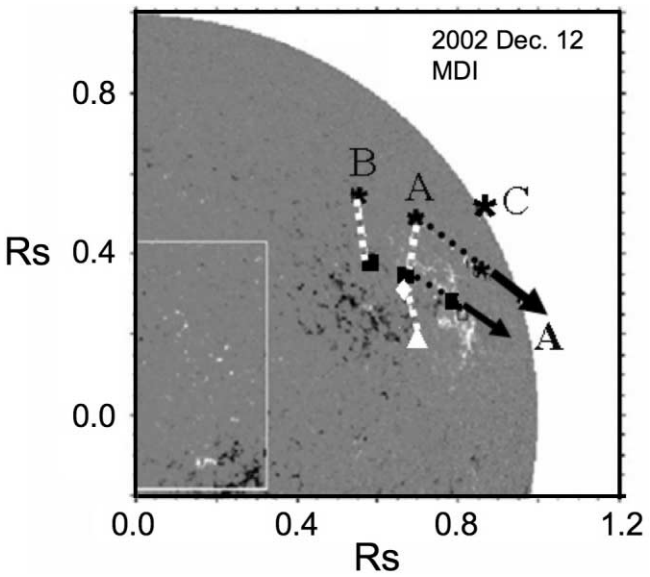

FIG. 7.—Radio source motions for the 2002 December 12 event. Superposed on an MDI magnetogram are radio burst centroids measured at 164 (*asterisks*), 236 (*black squares*), 327 (*diamond*), and 410 (*triangle*) MHz. White dotted lines show the initial location of source A; later this source moved along the dotted lines at ~1500 km s^{-1} in the direction shown the by arrows. The locations of source B at two frequencies (connected by a white dotted line) and the location of source C are also shown.

W35° and AR 10212 at N15°, W55°). While the source was stationary, it was observed at different frequencies along the broken white line in the figure. After it began to move at 12:37 UT it followed the direction shown by the black arrows, with a speed of approximately 1500 km s^{-1}. This same direction of motion is indicated by the thick yellow arrow in the bottom right panel of Figure 4.

How can we interpret this complex behavior? Because these events are associated with jets of the kind studied by Wang & Sheeley (2002), we adapt their framework in which the photospheric evolution of the closed field lines causes them to reconnect with the overlying open field lines (Shimojo & Shibata 2000), allowing for the release of the trapped energy in the form of jetlike ejections and also of accelerated electrons. The first packet of apparently stationary type III bursts is attributed to these electrons. Less than a couple of minutes later, the electrons are injected in different directions producing the type III bursts observed at locations A, B, and C in Figure 7. We suggest that the electron acceleration during this phase is due to a coronal disturbance initiated in coincidence with the jet or narrow CME ejection, which then propagates along different directions (such as a wave disturbance, possibly generated by the CME itself; see Cliver et al. 1999). This disturbance then triggers magnetic interactions at different locations. The sources A are an indirect signature of this disturbance (and perhaps also the simultaneous decrease in the high-frequency cutoff of the type III bursts). The disturbance moves to progressively lower latitudes with a projected speed of 1000 km s^{-1}, consistent with onset times of sources B and C if we assume that they were initiated by the same disturbance. The electrons then escaped to produce the classic frequency pattern shown in the top panel of Figure 6. Even though the CME from this event was directed out of the ecliptic, the motion of the radio source toward the ecliptic makes it quite plausible that these electrons reached field lines connected to 1 AU and were responsible for the observed impulsive electron event.

Of course, this interpretation is speculative, but we believe it is plausible. Our main point here is that although ^{3}He-rich impulsive flares are believed to come from compact sites in the corona, the associated type III emission in events such as 2002 December 12 can arise from a much more sizeable region where electron acceleration on both open and closed field lines is associated with the propagation of a disturbance that covers tens of degrees of heliolongitude.

2.4. *Energetic Particle Injection Times*

The injection times of the >15 MeV protons and ≥13 keV electrons shown in Table 1 are all within a few minutes of each other, and all correspond closely to the type III burst times. Although the low-energy ion injection times have large uncertainties, they tend to be later than the electrons. It is important to note that in some of the events in Table 1, the ^{3}He-rich SEPs were observed essentially continuously over a longer period, and the cited injections took place within this longer period. Specifically, ongoing ^{3}He enrichments were observed from periods 2002 October 5–7, October 20–22, and December 11–13. During these periods recurrent jets and/or narrow CMEs were observed as shown in Paper I. For example, we have examined the 2002 October 20–22 period to see if these jets were consistently associated with type III bursts; as shown in Figure 8, for every jet that occurred during the viewing hours of the NRH, a type III burst was seen in the same general area as the jets (impulsive electron events were also seen by the *Wind* instrument associated with these three bursts). The long-term presence of

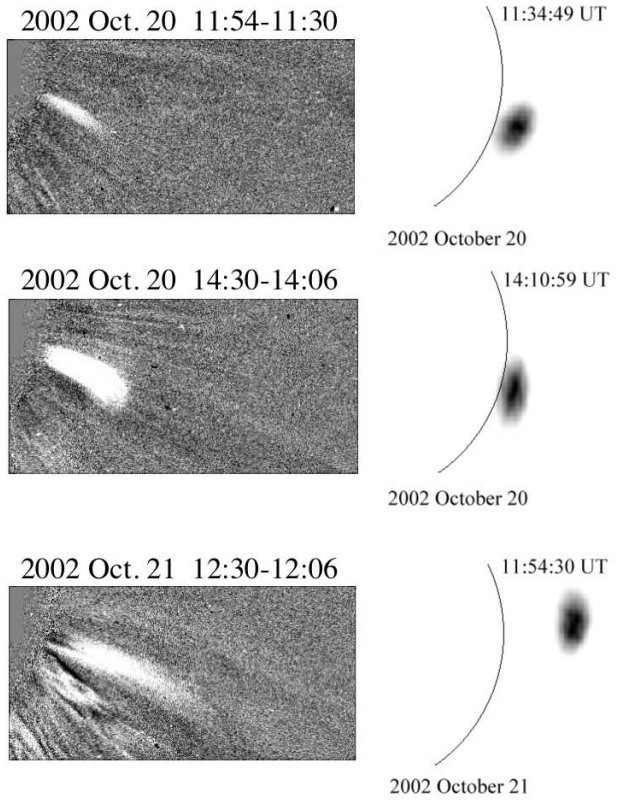

FIG. 8.—*Left*: Recurrent LASCO EIT jets from the active region that produced event 3. Each of these jets was associated with a type III burst, whose location is shown in the right panels.

^{3}He and optical data showing multiple jets during these periods is shown in Paper I. These longer periods suggest that there is quasi-steady acceleration of ^{3}He-enriched material associated with these active regions.

3. DISCUSSION

This study of the source regions of six ^{3}He-rich impulsive SEP events using radio imaging and timing, energetic particle timing, and EUV and white-light observations accompanied by PFSS model calculations of the coronal magnetic field confirms the identifications from Paper I. The sources are small active regions that show sporadic EUV brightenings or jets that appear to be the counterparts of white-light ejections. The source regions are located inside or at the boundary regions of open field line regions (coronal holes) between W33° and W65°. The activity observed in these regions is similar to jets identified by Wang & Sheeley (2002).

These events are accompanied by fast (700–1000 km s^{-1}) and narrow white-light ejections (see also Kahler 2001). The jets and/or narrow CMEs are often directed as much as 40° out of the ecliptic plane. The injected energetic particles can promptly reach 1 AU by following field lines that connect the source region to the ecliptic plane, and so they are not constrained to follow the same trajectory as the bulk of the CME (see also Maia et al. 2001). In Paper I, which included the events studied here, we concluded that the SEPs originated at the interface between active regions and small coronal holes. EUV jets observed in this kind of region are interpreted as due to magnetic reconnection between the active region and the open flux from the coronal hole (Shimojo & Shibata 2000; Kahler et al. 2001; Wang & Sheeley 2002). This scenario is consistent with the spatial coincidence of

the type III radio bursts with the X-ray and EUV jets (Kundu et al. 1995; Raulin et al. 1996). In some cases we observe multiple sources above the active region (see also Raoult & Pick 1980; Trottet et al. 1982).

The type III radio bursts of four of the six events showed simple features. Two events, 1 and 4, were more complex; they had type III sources that moved with speeds exceeding 1000 km s^{-1}, and the high-frequency cutoff of the type III bursts progressively moved toward lower frequencies. In these events one can distinguish two successive phases in the electron acceleration process responsible for the type III bursts: the type III source is stationary in the first phase, and in the second phase the type III sources move in a manner suggestive of a wavelike disturbance. Krucker et al. (1999) observed that in some impulsive electron events the >25 keV electrons are released up to half an hour later than the type III burst onsets. They concluded that the electrons were more likely related to propagating coronal transient waves (identified in EUV as EIT waves or Moreton waves) than to the flare itself. A similar conclusion was reached by Pick et al. (2003) and Maia & Pick (2004) from a study of "radio complex" events, in which it was found that the release time of electrons was delayed from the type III burst onsets and frequently coincided with the appearance of type II–like onsets, i.e., shocks (and/or broad continua) accompanied by type III production. The simplest proposed explanation for the origin of the particles is the coronal magnetic interaction, which also gives rise to these radio signatures. Events 1 and 4 appear rather similar to these types of events: the main difference being that the stationary and moving phases of the type III burst are separated by a shorter timescale (<2 minutes).

Since small bipoles are continually emerging inside coronal holes, the reconnection mechanism can occur over extended periods, thus leading to the nearly long-lasting and nearly continuous injection of ^{3}He and Fe-rich SEPs (Paper I). This may account for the fact that energetic ^{3}He is almost continuously present in the interplanetary medium at 1 AU during solar active periods, even when no obvious injections are taking place (Wiedenbeck et al. 2005).

In a careful study of 11 impulsive events (that included events 2 and 3 from this work), Wang et al. (2005) found that $\sim$1 MeV nucleon^{-1} ions were injected an average of 1.23 $\pm$ 0.24 hr after the $\leq$6 keV electrons, and 0.85 $\pm$ 20 hr after the $\geq$13 keV electrons. The associated CME altitude at this time was 4.22 $\pm$ 0.74 Rs. If the low-energy ions were accelerated at this very high altitude in the corona, then the high-ionization states found in ^{3}He-rich events are difficult to achieve either through stripping (Klecker et al. 1984; Reames et al. 1999; Barghouty & Mewaldt 2000; Möbius et al. 2003; Kartavykh et al. 2005; Dröge et al. 2006) or by ionization in the $\sim$10 MK plasma required to explain the high charge states (e.g., Reames et al. 1994). An additional problem with a CME associated acceleration scenario for the ions is the fact that the optical data show the CME is narrow in width and directed generally away from the ecliptic, and so the energetic particles could be expected to have poor or no magnetic connection to the observer at 1 AU, while in fact prompt access is observed (see also Reames 2002).

Conceivably the delay in the low-energy ion arrivals is caused by scattering between the source and 1 AU, but this cannot be tested with the available data. Nevertheless, given that the jet events typically last only 10–20 minutes, and that the electrons, 15 MeV protons, and type III bursts occur within 5–10 minutes of each other, it seems hard to understand what process would inject the low-energy ions an hour later, especially in a location where there appears to be no candidate mechanism to achieve the observed high-ionization states. We believe that the scenario that is most consistent with all the data is the one suggested by Paper I: that the activity associated with jets is the likely source of the particle events, and that the electrons and ions are accelerated at a time close to the jet. Although the CMEs in these events are narrow and generally directed well off the ecliptic plane, the ions and electrons that are observed at 1 AU reach the ecliptic along field lines such as those shown in the PFSS calculations. Some type III bursts may be due to electron beams that remain trapped or that escape but do not reach Earth, so it is not possible in detail to systematically associate the type III bursts with events that reach Earth.

For the ^{3}He-enrich energetic ions, it is important to remember that the CME-associated events in this study are unusual for this kind of SEP event, and so the properties of this set of events may not be typical. It will be important to investigate the relationship of complex radio events (Maia & Pick 2004) to ^{3}He-rich events. The radio data analysis in this study took account of spectral and spatial evolution of the radio emission, but had limited spectral coverage, and imaging data only at metric wavelengths. The high cadence of the radio imaging measurements (<a few seconds) made it possible to observe the spatial and temporal development of these short-duration impulsive events. Future observations with improved radio observations and higher cadence optical and multispacecraft energetic particle measurements should give much improved characterizations of the impulsive events studied here, and perhaps also the nearly steady multiday emissions of energetic ^{3}He often observed at 1 AU.

We thank the EIT, LASCO, and MDI teams for their observational data. The NSO Kitt Peak data used for the magnetograms were produced cooperatively by NSF NOAO, NSAS GSFC, and NOAA SEC. We are grateful to P. Démoulin, D. Maia, and S. Pohjolainen for very helpful discussions and suggestions. This research was supported by NASA at JHU APL by grant NNG 04-GJ51G, and at Berkeley by grant NNG 05-GH18G and ONR NRL. The two visits of C. Tan in the Paris Observatory were supported by the Chinese Academy of Sciences (CAS) and CNRS through the French-Chinese cooperation and by the Paris Observatory. We acknowledge financial support by the CNES.

REFERENCES

Barghouty, A. F., & Mewaldt, R. A. 2000, in AIP Conf. Proc. 528, Acceleration and Transport of Energetic Particles Observed in the Heliosphere, ed. R. A. Mewaldt et al. (Melville: AIP), 71
Bougeret, J. L., et al. 1995, Space Sci. Rev., 71, 231
Brueckner, G. E., et al. 1995, Sol. Phys., 162, 357
Cliver, E. W., Webb, D. F., & Howard, R. A. 1999, Sol. Phys., 187, 89
Delaboudinière, J.-P., et al. 1995, Sol. Phys., 162, 291
Dröge, W., Kartavykh, J. J., Klecker, B., & Mason, G. M. 2006, ApJ, 645, 1516
Garrard, T. L., Stone, E. C., & Vogt, R. E. 1973, in High Energy Phenomena on the Sun, ed. R. Ramaty & R. G. Stone (NASA SP-342; Washington: NASA), 341
Geiss, J., & Reeves, H. 1972, A&A, 18, 126
Gold, R. E., et al. 1998, Space Sci. Rev., 86, 541
Hsieh, K. C., & Simpson, J. A. 1970, ApJ, 162, L191
Kahler, S. W. 2001, J. Geophys. Res., 106, 20947
Kahler, S. W., Reames, D. V., & Sheeley, N. R., Jr. 2001, ApJ, 562, 558
Kartavykh, J. J., Dröge, W., Kovaltsov, G. A., & Ostryakov, V. M. 2005, Sol. Phys., 227, 123
Kerdraon, A., & Delouis, J.-M. 1997, in Coronal Physics from Radio and Space Observations, ed. G. Trottet (Berlin: Springer), 192
Klecker, B., et al. 1984, ApJ, 281, 458

Klein, K. L., & Posner, A. 2005, A&A, 438, 1029
Krucker, S., Larson, D. L., Lin, R. P., & Thompson, B. J. 1999, ApJ, 519, 864
Kundu, M. R., Raulin, J. P., Pick, M., & Strong, K. T. 1995, ApJ, 444, 922
Lecacheux, A. 2000, in Radio Astronomy at Long Wavelengths, ed. R. G. Stone et al. (Geophys. Monogr. 119; Washington: AGU), 321
Lin, R. P., et al. 1995, Space Sci. Rev., 71, 125
Maia, D., & Pick, M. 2004, ApJ, 609, 1082
Maia, D., Pick, M., Hawkins, S. E. I., & Krucker, S. 2001, ApJ, 560, 1058
Mann, G., Aurass, H., Voigt, W., & Paschke, J. 1992, in Coronal Streamers, Coronal Loops, and Coronal and Solar Wind Composition, ed. C. Mattok (ESA SP-348: Paris: ESA), 129
Mason, G. M., Dwyer, J. R., & Mazur, J. E. 2000, ApJ, 545, L157
Mason, G. M., et al. 1998, Space Sci. Rev., 86, 409
———. 2002, ApJ, 574, 1039
———. 2004, ApJ, 606, 555
Möbius, E., et al. 2003, Proc. 28th Int. Cosmic-Ray Conf. (Tsukuba), 3273
Pick, M., Maia, D., Wang, S. J., Lecacheux, A., & Hawkins, S. E. 2003, Adv. Space Res., 32, 2527
Raoult, A., & Pick, M. 1980, A&A, 87, 63
Raulin, J. P., Kundu, M. R., Hudson, H. S., Nitta, N., & Raoult, A. 1996, A&A, 306, 299
Reames, D. V. 1996, in AIP Conf. Ser. 374, High Energy Solar Physics, ed. R. Ramaty, N. Mandzhavidze, & X.-M. Hua (Woodbury: AIP), 35
———. 2002, ApJ, 571, L63
Reames, D. V., Dennis, B. R., Stone, R. G., & Lin, R. P. 1988, ApJ, 327, 998
Reames, D. V., Meyer, J. P., & von Rosenvinge, T. T. 1994, ApJS, 90, 649
Reames, D. V., Ng, C. K., & Tylka, A. J. 1999, Geophys. Res. Lett., 26, 3585
Reames, D. V., von Rosenvinge, T. T., & Lin, R. P. 1985, ApJ, 292, 716
Scherrer, P. H., et al. 1995, Sol. Phys., 162, 129
Serlemitsos, A. T., & Balasubrahmanyan, V. K. 1975, ApJ, 198, 195
Shimojo, M., & Shibata, K. 2000, ApJ, 542, 1100
Stone, E. C., et al. 1998, Space Sci. Rev., 86, 1
Trottet, G., Pick, M., House, L., Illing, R., Sawyer, C., & Wagner, W. 1982, A&A, 111, 306
Wang, L., Lin, R. P., Krucker, S., & Mason, G. M. 2005, in Proc. Solar Wind 11/*SOHO* 16, Connecting Sun and Heliosphere (Noordwijk: ESA), SH33A-01
Wang, Y.-M., Pick, M., & Mason, G. M. 2006, ApJ, 639, 495 (Paper I)
Wang, Y.-M., & Sheeley, N. R. 2002, ApJ, 575, 542
Wiedenbeck, M. E., et al. 2005, Proc. 29th Int. Cosmic-Ray Conf. (Pune), SH34A-03